Int Nano Lett (2015) 5:101–107
DOI 10.1007/s40089-015-0143-x

ORIGINAL ARTICLE

Lanthanum cerate ($La_2Ce_2O_7$): hydrothermal synthesis, characterization and optical properties

Shahin Khademinia · Mahdi Behzad

Received: 10 December 2014 / Accepted: 19 February 2015 / Published online: 3 March 2015

Abstract $La_2Ce_2O_7$ nano-powders were synthesized via a hydrothermal reaction in a deionized water (S_1) and in a 2 M NaOH aqueous solution (S_2) at 180 °C for 48 h. $La(NO_3)_3{\cdot}H_2O$ and $(NH_4)_2Ce(NO_3)_6$ were used in the stoichiometric 1:1 La:Ce molar ratio as raw materials. The obtained materials were crystallized in a cubic crystal structure with space group. The synthesized materials were characterized by powder X-ray diffraction technique and Fourier-transform infrared spectroscopy. To investigate the effect of the basic solution on the morphology of the obtained materials, the morphologies of the synthesized materials were studied by field emission scanning electron microscopy technique. The technique showed that the morphology of $La_2Ce_2O_7$ samples changed from grain to rod-like structure in presence of the basic solution. Cell parameter refinements showed that these parameters were larger for S_2 than those for S_1. Photoluminescence and ultraviolet visible spectra of the synthesized nanomaterials were also investigated.

Keywords $La_2Ce_2O_7$ · Hydrothermal · Nano materials · PXRD

S. Khademinia · M. Behzad (✉)
Department of Chemistry, Semnan University,
Semnan 35351-19111, Iran
e-mail: mbehzad@semnan.ac.ir; mahdibehzad@gmail.com

S. Khademinia
e-mail: shahinkhademinia@gmail.com

Introduction

There is a great interest in pyrochlore materials due to their unique applications such as in catalysis [1–4], electronic [5], optical [6] magnetic properties [7] and solid oxide fuel cells (SOFC) [8]. Among them, oxides and fluorites with general formula $A_2B_2O_7$ (where A is a medium-large cation and B is an octahedrally coordinated, high-charge cation) have attracted considerable attention [9]. Lanthanum cerate, $La_2Ce_2O_7$, has been studied as an oxide ion conductor [10], electrode component in proton conducting fuel cells [11], and hydrogen permeation membranes [12]. $La_2Ce_2O_7$ has also shown appreciable proton conductivity under reduced atmosphere as well as satisfactory stability in the presence of CO_2. These virtues have made $La_2Ce_2O_7$ a potentially promising electrolyte for solid oxide fuel cells and a possible outstanding candidate as a hydrogen separation membrane [13–15]. Several methods such sol–gel method [16], citrate co-precipitation route [17], alkaline solid-state reaction [12], conventional hydrothermal method at 180 °C for 24 h [18], solution reaction method [19], pressure-less sintering sol–gel at 1600 °C for 10 h [20], atmospheric plasma spraying (APS) techniques [21] EDTA-citric acid complexation process [22], electron beam-physical vapor deposition (EB-PVD) [23] hydrothermal method using polyethylene glycol at 180 °C for 24 h [24], high temperature solid state [25], air plasma spraying [26] have previously been reported for the synthesis of $La_2Ce_2O_7$. In the present study, a hydrothermal route has been successfully employed for the synthesis of nanostructured $La_2Ce_2O_7$ using $La(NO_3)_3{\cdot}H_2O$ and $(NH_4)_2Ce(NO_3)_6$ as raw materials in deionized water (S_1) and 2 M NaOH (S_2). Cell parameter refinements, Fourier-transform infrared spectroscopy (FTIR), photoluminescence and ultraviolet visible spectra of the synthesized nanomaterials were also investigated.

Experimental

Materials and methods

All chemicals were of analytical grade, obtained from Merck Company and used without further purification. Phase identifications were performed on a powder X-ray diffractometer D5000 (Siemens AG, Munich, Germany) using CuKα radiation. The morphology of the obtained materials was examined with a field emission scanning electron microscope (Hitachi FE-SEM model S-4160). Absorption and photoluminescence spectra were recorded on a Analytik Jena Specord 40 (Analytik Jena AG Analytical Instrumentation, Jena, Germany) and a Perkin Elmer LF-5 spectrometer (Perkin Elmer Inc., Waltham, MA, USA), respectively. FT-IR spectra were recorded on a Tensor 27 instrument (Bruker Corporation, Germany). Cell parameter refinements were also reported by celref software version 3.

Typical procedure for the synthesis of $La_2Ce_2O_7$

In a typical synthetic experiment, 0.32 g (0.98 mmol) of $La(NO_3)_3{\cdot}H_2O$ ($M_w = 324.92\ gmol^{-1}$) and 0.54 g (0.98 mmol) of $(NH_4)_2Ce(NO_3)_6$ ($M_w = 548.32\ gmol^{-1}$) were added to 50 mL of deionized water (S_1) or 50 mL of hot aqueous solution of 2 M NaOH(S_2) under magnetic stirring at 80 °C. The resultant solution was stirred for further 15 min and then transferred into a 100 mL Teflon lined stainless steel autoclave. The autoclave was sealed and heated at 180 °C for 48 h. When the reaction was completed, it was cooled down to room temperature by water immediately. The prepared powders were washed with deionize water and dried at 120 °C for 20 min under normal atmospheric conditions and creamlike powders were collected.

Result and discussion

Powder X-ray diffraction analysis (PXRD)

Tables 1 and 2 show the crystallographic data of the S_1 and S_2, respectively. The data in Table 1 shows the XRD peaks in the range of $2\theta = 4°–70°$. The five intensive peaks that are corresponded to the pure $La_2Ce_2O_7$ phase are in agreement with the literature [12, 17–19]. As shown in Table 2, there are five peaks similar to those of Table 1 that are corresponded to the pure $La_2Ce_2O_7$. However, there is a blue shift in the 2θ values indicating an expansion in the unit cell of S_2 compared to S_1. Besides, there are several additional XRD peaks at around 15.77°, 27.41°, 31.73°, 48.72° and 54.23° which are related to La_2O_3 [27–29]. Comparison of the data in Tables 1 and 2 show that by changing the conditions from deionized water to basic solution the crystals' growth has increased but the material was not obtained as a pure phase.

Table 1 Crystallographic data for S_1

Entry	2θ	d (interplanar spacing)	Intensity (counts)	Miller indices (hkl)
1	28.62	3.12	347	111
2	32.72	2.73	145	200
3	47.04	1.93	155	220
4	56.27	1.63	122	311
5	57.41	1.60	74	222

Table 2 Crystallographic data for S_2

Entry	2θ	d (interplanar spacing)	Intensity
1	15.72	5.62	271
2	27.41	3.25	260
3	28.11	3.171	368
4	31.68	2.81	108
5	32.35	2.76	87
6	39.60	2.27	187
7	47.35	1.91	100
8	48.72	1.86	184
9	54.20	1.68	64
10	56.37	1.63	100

Table 3 Cell parameter refinements of S_1 and S_2

Cell parameter	a (Å)	Volume (Å^3)
Standard	5.570	172.809
S_1	5.4198	159.20
Standard deviation	0.0814	2.392
S_2	5.6061	176.19
Standard deviation	0.1932	6.073

Table 3 shows the cell parameter refinement data of the obtained materials. It is clear that with changing the solution pH, the parameter a was increased and so there was an expansion in the unit cell. The data were in good agreement with the interplanar spacing calculated by a Bragg's equation. Besides, Table 3 shows the standard deviations of the cell parameters and cell volume for S_1 and S_2. It shows that the values are small enough until we can compare the a parameter and volume value for S_1 and S_2 without doubt.

The crystal phases of the hydrothermally synthesized nanomaterials at 180 °C for 48 h in deionized water and aqueous NaOH solutions were examined by powder X-ray

diffraction technique. Figure 1 shows the PXRD data which confirms that the $La_2Ce_2O_7$ was crystallized in a cubic crystal structure with Fd3-m space group. According to the PXRD data, it was clear that with using deionized water solution, the pure $La_2Ce_2O_7$ phase was prepared but when NaOH solution was used, there was a mixture of two phases namely $La_2Ce_2O_7$ and La_2O_3. Also, using the sharpest peak at hkl = 111, interplanar spacing was calculated using Bragg's equation as follows: $\Delta d = d(S_2) - d(S_1) = 3.171 - 3.117 = 0.054$ Å. So, it showed that with changing the reaction condition, there was an expansion in the unit cell. The crystal size of S_1 was calculated via Scherrer equation $t = \frac{k\lambda}{B_{\frac{1}{2}} \cos\theta}$ using the peak at $2\theta = 32.72°$ (Table 1). In this equation, t is the entire thickness of the crystalline sample, λ is the x-ray diffraction wavelength (0.154 nm), and k is the Scherrer constant (0.9); $B_{1/2}$ of FWHM is the full width at half its maximum intensity and θ (=16.37) is the half diffraction angle at which the peak is located. It was found that the calculated crystal size is 17 nm.

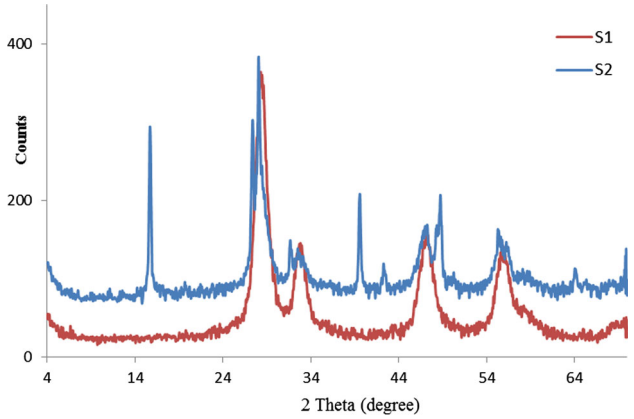

Fig. 1 PXRD patterns of the hydrothermally synthesized $La_2Ce_2O_7$ nanomaterials

Morphology analysis

Figure 2 represents the field emission scanning electron microscopy (FESEM) images of the synthesized $La_2Ce_2O_7$ nano materials. It is clear that the obtained materials are in grain structure. According to Fig. 2a–c, it is clear that the morphology of the obtained materials is homogeneous. Figure 2d shows that the size distribution of the obtained materials is also homogeneous. As shown in the figure, it is clear that the diameter size of the grain nanostructures is about 30–50 nm.

Figure 3 represents the FESEM images of the synthesized $La_2Ce_2O_7$ nanomaterials. It shows that with changing the reaction condition and using basic solution instead of deionize water, the morphology of the obtained materials were changed from non-homogeneous grain-like structures to non-homogeneous rod structures. Figure 3a, b shows

Fig. 2 FESEM images of S_1

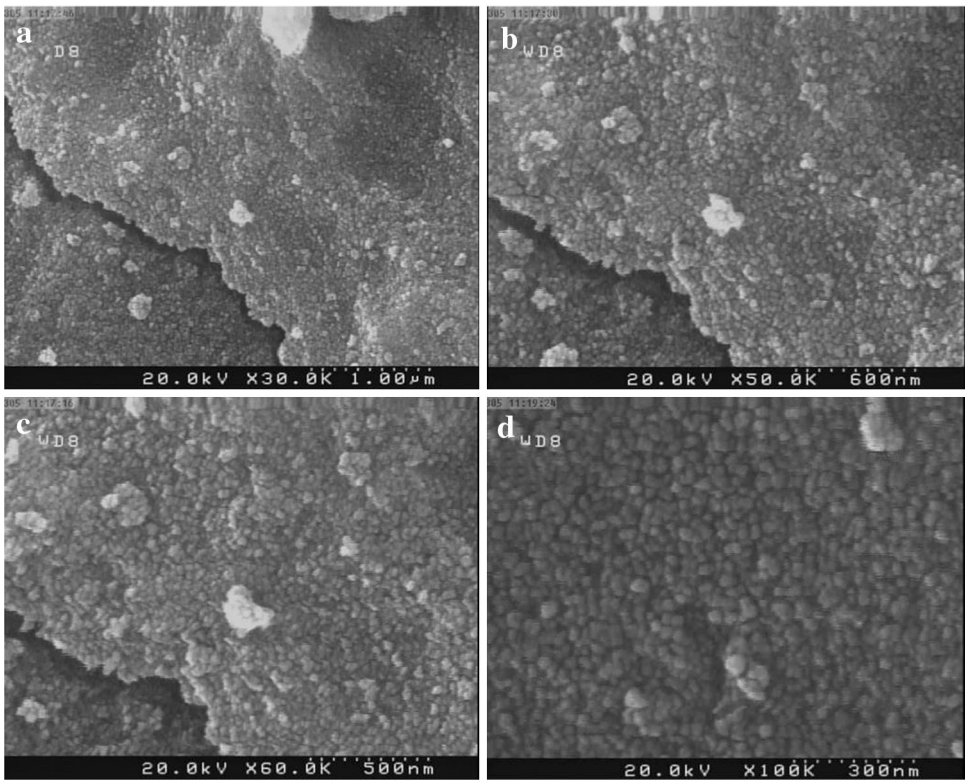

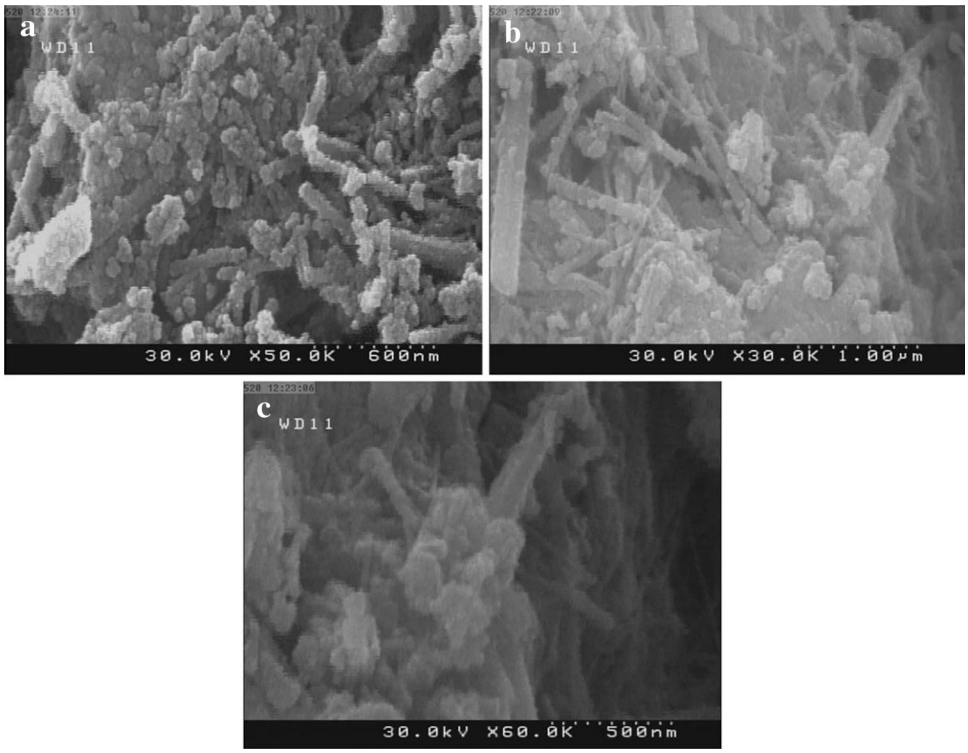

Fig. 3 FESEM images of S_2

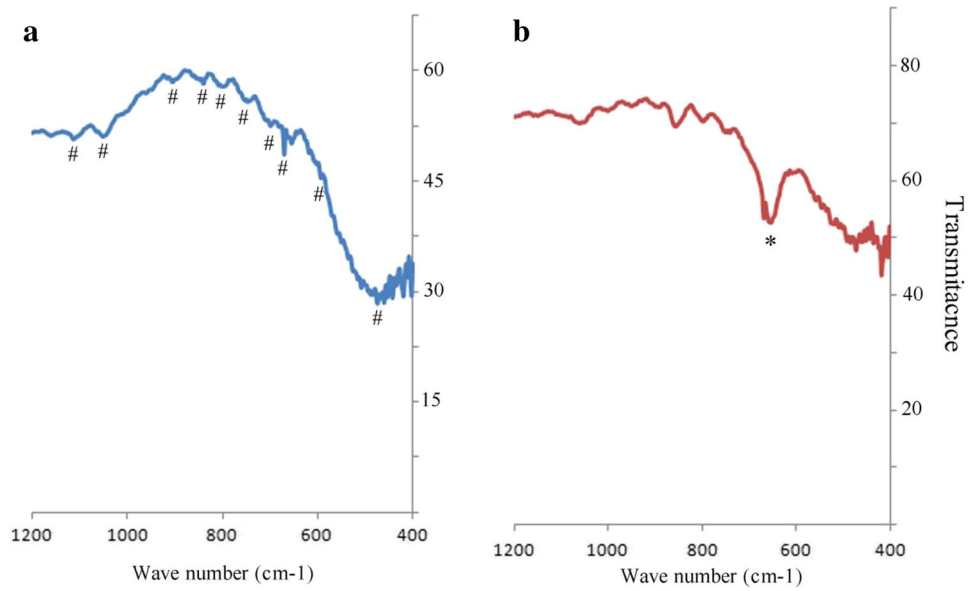

Fig. 4 The FTIR spectra of S_1 and S_2. *Asterisk* is due to the presence of La_2O_3 and *hash* is the peak positions

that the morphology of the obtained materials are a mixture of rod and particle structures that according to the XRD pattern, it might be due to the existence of two phases in the obtained material. As shown in Fig. 3b, it is clear that the size of the obtained materials is non-homogeneous and the length size of the rod structures is between 700 nm–1.5 µm and the thickness size of the materials is about 60–100 nm. However, it was found that there was bulk materials formed via the process condition. It confirmed the incomplete phase formation according to the PXRD patterns shown in Fig. 1.

Optical properties

Figure 4 shows the FTIR spectra of $La_2Ce_2O_7$ nano-powders in the wave number range of 400–1200 cm^{-1}. Several

characteristic absorption bands can be observed at about 472, 592, 653.82, 669, 698, 752, 794, 838, 904, 1051 and 1112 cm^{-1}. As shown in Fig. 4b, there is a peak at 653 cm^{-1} which could be attributed to the presence of free La_2O_3 and its La–O stretching vibrations [27]. The signals are in agreement with previously reported FTIR data for $La_2Ce_2O_7$.

Figure 5a, b show the photoluminescence (pL) spectra of S_1 and S_2, respectively. As seen in Fig. 5a, there are some peaks at about 480, 510; a weak peak at about 590 and a broad and intensive peak at 650–750 nm. Figure 5b also shows peaks at about 490, 530, 610 and a shoulder at about 650–720 nm. The broad and intensive peak at 650–750 nm in Fig. 5a is due to the oxygen deficiency in the crystal structure which is typical of the $A_2B_2O_7$ pyrochlores. Figure 5b also shows similar band at this region, but this band is much weaker which means that S_2 is not a pure $La_2Ce_2O_7$ phase. These data are in accordance with the PXRD data [30, 31].

Figure 6a shows the ultraviolet visible spectra (UV–Vis) spectrum of S_1. Two main absorption bands could be observed at around 240 and 295 nm. The calculated band gap using the absorption edge for S_1 was 3.1 eV which is lower than the band gap of pure CeO_2 (3.5 eV) [30, 31]. Figure 6b shows only one peak at about 265 nm which is different from that of S_1. These data also confirm that S_2 is not a pure pyrochlore structure.

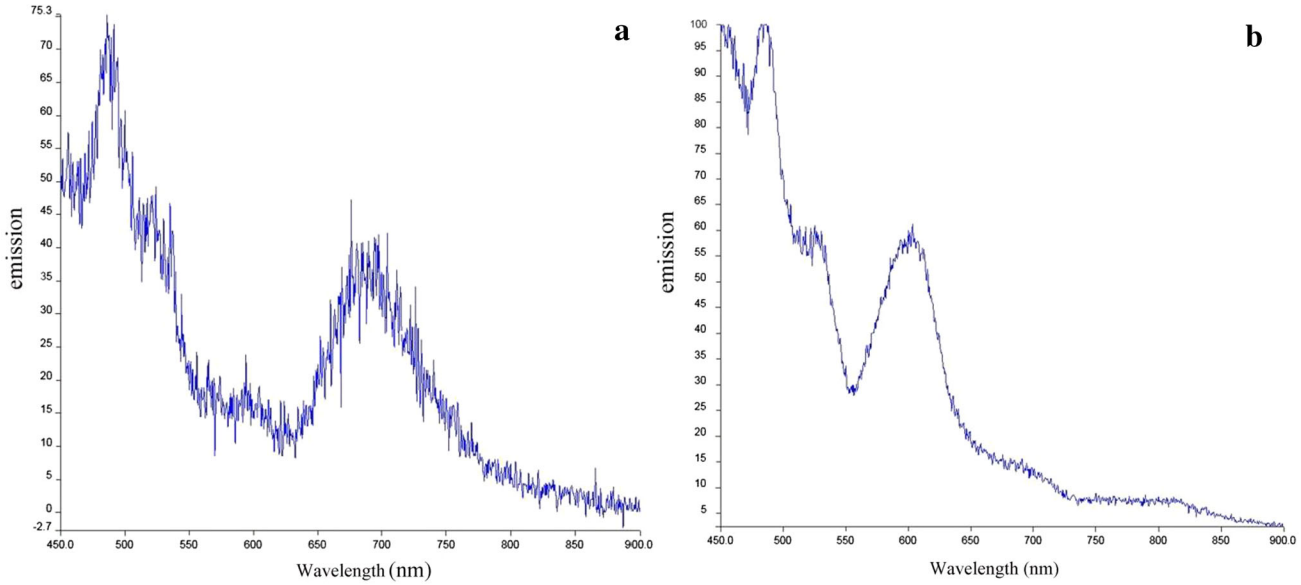

Fig. 5 The pL spectra of **a** S_1 ($\lambda_{ex} = 200$ nm) and **b** S_2($\lambda_{ex} = 200$ nm)

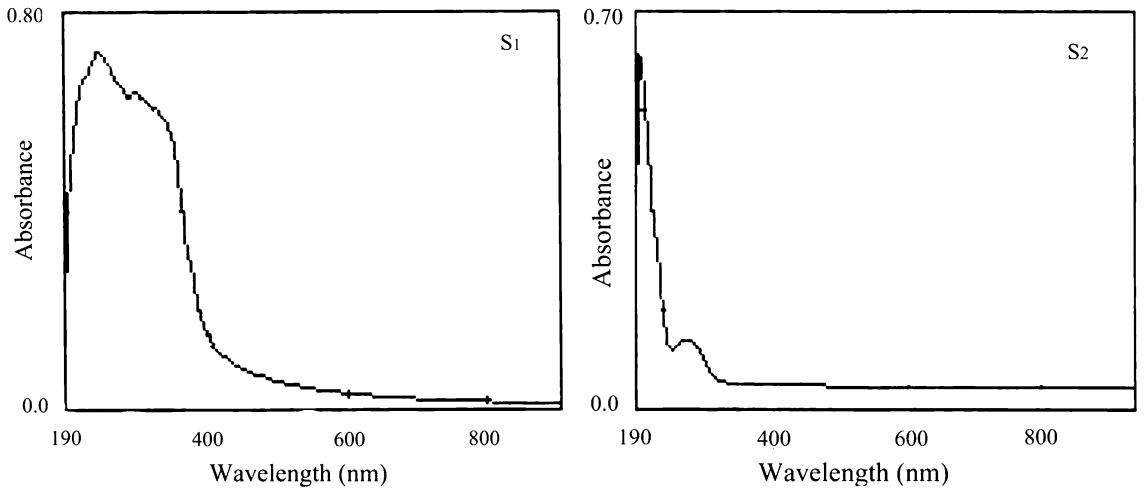

Fig. 6 The UV–Vis spectrum of S_1

Conclusion

In this research work, $La_2Ce_2O_7$ grain and rod nanomaterials were synthesized successfully via mild condition hydrothermal methods. PXRD patterns showed that the synthesis was performed successfully. It showed that the crystal growth for S_2 was better than that for S_1. However, it showed that the phase purity of S_1 was complete, but S_2 was a mixture of two phases of $La_2Ce_2O_7$ and La_2O_3. FESEM images showed that the as-synthesized nanomaterials were in grain and rod structures. It showed that the average particle sizes of S_2 were larger than those of S_1 that were in good agreement with those of XRD and cell parameter data. Optical properties of the synthesized nanomaterials were also investigated. FTIR spectra confirmed that the synthesis procedure was complete for S_1 and there was free La_2O_3 peaks for S_2. pL and UV–Vis spectroscopy also showed the characteristic emission and absorption peaks of $A_2B_2O_7$ pyrochlores which confirmed the successful synthesis of $La_2Ce_2O_7$ nanomaterials.

References

1. Thomson, J.B., Armstrong, A.R., Bruce, P.G.: An oxygen-rich pyrochlore with fluorite composition. J. Solid State Chem. **148**, 56–62 (1999)
2. Kishimoto, H., Omata, T., Otsuka-Yao-Matsuo, S., Ueda, K., Hosono, H., Kawazoe, H.: Crystal structure of metastable κ-$CeZrO_4$ phase possessing an ordered arrangement of Ce and Zr ions. J. Alloys Compd. 312, 94–10 (32000)
3. Haynes, D.J., Berry, D.A., Shekhawat, D., Spivey, J.J.: Catalytic partial oxidation of *n*-tetradecane using pyrochlores: effect of Rh and Sr substitution. Catal. Today **136**, 206–213 (2008)
4. Kieffer, R., Fujiwara, M., Udron, L., Souma, Y.: Hydrogenation of CO and CO_2 toward methanol, alcohols and hydrocarbons on promoted copper-rare earth oxides catalysts. Catal. Today **36**, 15–24 (1997)
5. Matsuhira, K., Wakeshima, M., Hinatsu, Y., Takagi, S.: J. Phys. Soc. Jap. 80 (2011)
6. Brik, M.G., Srivastava, A.M., Avram, N.M.: Enhanced phytoremediation potential of polychlorinated biphenyl contaminated soil from e-waste recycling area in the presence of randomly methylated-[beta]-cyclodextrins. Opt. Mater. **33**, 1671–1676 (2011)
7. Ross, K.A., Yaraskavitch, L.R., Laver, M., Gardner, J.S., Quilliam, J.A., Meng, S., Kycia, J.B., Singh, D.K., Proffen, T., Dabkowska, H.A., Gaulin, B.D.: Dimensional evolution of spin correlations in the magnetic pyrochlore $Yb_2Ti_2O_7$. Phys. Rev. B. **84**, 174442 (2011)
8. Gill, J.K., Pandey, O.P., Singh, K.: Ionic conductivity, structural and thermal properties of pure and Sr^{2+} doped $Y_2Ti_2O_7$ pyrochlores for SOFC. Solid State Sci. **13**, 1960–1966 (2011)
9. Yamamura, H.N.H., Nishino, H., Kakinuma, K., Nomura, K.: Crystal phase and electrical conductivity in the pyrochlore-type composition systems, $Ln_2Ce_2O_7$ (Ln=La, Nd, Sm, Eu, Gd, Y and Yb). J. Ceram. Soc. Jpn. **1300**, 902–906 (2003)
10. Lin, B., Wang, S.L., Liu, X.Q., Meng, G.Y.: Stable proton-conducting Ca-doped $LaNbO_4$ thin electrolyte-based protonic ceramic membrane fuel cells by in situ screen printing. J. Alloys Compd. **478**, 355 (2009)
11. Yan, L., Sun, W., Bi, L., Fang, S., Tao, Z., Liu, W.: Effect of Sm-doping on the hydrogen permeation of Ni–$La_2Ce_2O_7$ mixed protonic–electronic conductor. Int. J. Hydrogen Energy **35**, 4508 (2010)
12. Lopes, F.W.B., de Souza, C.P., de Morais, A.M.V., Dallas, J.P., Gavarri, J.R.: Determination of $RE_2Ce_2O_7$ pyrochlore phases from monazite–allanite ores. Hydrometallurgy **97**, 167–172 (2009)
13. Fang, S.M., Bi, L., Yan, L.T., Sun, W.P., Chen, C.S., Liu, W.: CO_2-resistant hydrogen permeation membranes based on doped ceria and nickel. J. Phys. Chem. C **114**, 10986–10991 (2010)
14. Tao, Z.T., Bi, L., Fang, S.M., Liu, W.: A stable $La_{1.95}Ca_{0.05}Ce_2O_{7-\delta}$ as the electrolyte for intermediate-temperature solid oxide fuel cells. J. Power Sources **195**, 3481–3484 (2010)
15. Zhu, Z.W., Yan, L.T., Liu, H.W., Sun, W.P., Zhang, Q.P., Liu, W.: A mixed electronic and protonic conducting hydrogen separation membrane with asymmetric structure. Int. J. Hydrogen Energy **37**, 12708–12713 (2012)
16. Weng, S.F., Wang, Y.H., Lee, C.S.: Autothermal steam reforming of ethanol over $La_2Ce_{2-x}Ru_xO_7$ ($x = 0$–0.35) catalyst for hydrogen production. Appl. Catal. B **134–135**, 359–366 (2013)
17. Besikiotis, V., Knee, C.S., Ahmed, I., Haugsrud, R., Norby, T.: Crystal structure, hydration and ionic conductivity of the inherently oxygen-deficient $La_2Ce_2O_7$. Solid State Ion. **228**, 1–7 (2012)
18. Wang, Y., Wang, C., Li, C., Cheng, Y.L., Chi, F.: Influence of different surfactants on crystal growth behavior and sinterability of $La_2Ce_2O_7$ solid solution. Ceram. Inter. **40**, 4305–4310 (2014)
19. Song, Z.H., Ge, C.X., Gang, L., Li, W.X., dan, D.X.: Influence of Gd_2O_3 addition on thermophysical properties of $La_2Ce_2O_7$ ceramics for thermal barrier coatings. J. Eur. Ceram. Soc. 32, 3693–3700 (2012)
20. Song, Z.H., Yuan, W., Gang, L., Ge, C.X., Li, W.X.: Investigation about thermal conductivities of $La_2Ce_2O_7$ doped with calcium or magnesium for thermal barrier coatings. J. Alloys Compd. **537**, 141–146 (2012)
21. Ma, W., Dong, H., Guo, H., Gong, S., Zheng, X.: Thermal cycling behavior of $La_2Ce_2O_7$/8YSZ double-ceramic-layer thermal barrier coatings prepared by atmospheric plasma spraying. Sur. Coat. Tech. **204**, 3366–3370 (2010)
22. Ling, Y.H., Zhang, X.Z., Wang, S.L., Zhao, L., Lin, B., Liu, X.Q.: A cobalt free $SrFe_{0.9}Sb_{0.1}O_3$-d cathode material for proton-conducting solid oxide fuel cells with stable $BaZr_{0.1}Ce_{0.7}Y_{0.1}Yb_{0.1}O_3$-d electrolyte. J. Power Sources **195**, 7042–7045 (2010)
23. Ma, W., Gong, S., Li, H., Xu, H.: Novel thermal barrier coatings based on $La_2Ce_2O_7$/8YSZ double-ceramic-layer systems deposited by electron beam physical vapor deposition. Sur. Coat. Tech. **202**, 2704–2708 (2008)
24. Wang, C., Huang, W., Wang, Y., Cheng, Y., Zou, B., Fan, X., Yang, J., Cao, X.: Synthesis of monodispersed $La_2Ce_2O_7$ nanocrystals via hydrothermal method: a study of crystal growth and sintering behavior. Int. J. Refract Metals Hard Mater. **31**, 242–246 (2012)
25. Bae, J.S., Choo, W.K., Lee, C.H.: The crystal structure of ionic conductor $La_xCe_{1-x}O_{2-x/2}$. J. Eur. Ceram. Soc. **24**, 1291–1294 (2004)
26. Ma, W., Ma, Y., Gong, S., Xu, H., Cao, X.: Thermal cycling behavior of lanthanum-cerium oxide thermal barrier coatings prepared by air plasma spraying. High-performance ceramics IV, PTS 1-3. Key Eng. Mater. **336–338**, 1759–1761 (2007)

27. Méndez, M., Carvajal, J.J., Cesteros, Y., Aguiló, M., Díaz, F., Giguère, A., Drouin, D., Martínez-Ferrero, E., Salagre, P., Formentín, P., Pallarès, J., Marsal, L.F.: Sol–gel Pechini synthesis and optical spectroscopy of nanocrystalline La_2O_3 doped with Eu^{3+}. Opt. Mater. **32**, 1686–1692 (2010)
28. Liu, X., Yan, L., Zou, J.: Tunable cathodoluminescence properties of Tb^{3+}-doped La_2O_3 nanocrystalline phosphors. J. Electrochem. Soc. **157**, P1–P6 (2010)
29. Hu, B.C., Liu, H., Dong, W., Zhang, Y., Bao, G., Lao, C., Wang, Z.L.: $La(OH)_3$ and La_2O_3 nanobelts—synthesis and physical properties. Adv. Mater. **9**, 470–474 (2007)
30. Li, L., Bing, Y.: CeO_2–Bi_2O_3 nanocomposite: two step synthesis, microstructure and photocatalytic activity. J. Non-Cryst. Sol. **355**, 776–779 (2009)
31. Ansari, A.A., Singh, S.P., Malhotra, B.D: Optical and structural properties of nanostructured CeO_2:Tb^{3+} film. J. Alloy Compd. 509, 262–265 (2011)